Oriented granulometry to quantify fibre orientation distributions in synthetic and plant fibre composite preforms

C. Vangsøe, N. Nørskov, M. Devaux, Estelle Bonnin, K. Bach Knudsen

HAL Id: hal-03162857
https://hal.inrae.fr/hal-03162857

Submitted on 22 Aug 2022

1 **Oriented granulometry to quantify fibre orientation distributions in synthetic and**

2 **plant fibre composite preforms**

3

4 Victor Gager [1,2], David Legland [3], Alain Bourmaud [1], Antoine Le Duigou [1], Floran Pierre

5 [2], Karim Behlouli [2], Christophe Baley [1]

6

7 [1] Univ. Bretagne Sud, UMR CNRS 6027, IRDL, F-56100 Lorient, France

8 [2] Eco-technilin SAS, ZA Caux Multipôles, 76190 Valliquerville, France

9 [3] UR1268 Biopolymères Interactions Assemblages, INRA, F-44316 Nantes, France

10 **Corresponding author: alain.bourmaud@univ-ubs.fr**

11

12 **Abstract**

13 Fibre orientation is an essential factor governing the mechanical properties of composite

14 materials. This study proposes an original method based on gray-level granulometry to

15 analyse the fibre orientation distribution (FOD) of synthetic and natural fibre

16 reinforcements aiming composite applications. An orientation maps is computed from

17 SEM images and frequency of fibre orientation is graphically illustrated for each

18 angular direction. First, glass fibre nonwoven and unidirectional preforms were

19 analysed as a model to validate the method before testing their flax fibre counterparts.

20 Differences in structural organisations were found between flax and glass fibre

21 reinforcement FOD due to the specific structure and mechanical behaviour of plant

22 fibres but also to the preform manufacturing process. Promising results were obtained

23 confirming the reliability of this novel numerical method for fibre orientation

24 determination.

25

1

1. Introduction

Flax fibres are now widely used as reinforcements for semi-structural and structural composite applications (Shah et al., 2013). Their specificities (low density, good mechanical properties, particular structure, low environmental impact, etc.) make them a very attractive alternative to synthetic fibres (Bourmaud et al., 2018). Flax fibres are commercially available for extrusion, injection moulding or as structured preforms for infusion and compression moulding such as unidirectional, multi-directional woven fabrics and also nonwoven mats. Selection of preforms can be managed depending on the properties and expected end applications. Nonwoven composites are mainly used in the automotive industry as interior parts because they combine good mechanical and acoustic properties (Merotte et al., 2016) but also thanks to their low manufacturing cost compared to fabrics. Composites performances are usually defined by the reinforcement, matrix and fibre/matrix interface properties (Jones, 1999). In terms of mechanical properties, additional parameters such as fibre volume ratio, fibre architecture and individualisation, porosity content as well as fibre orientation are of great importance. For this later, it is even more true when dealing with nonwoven biocomposites where the fibre orientation distribution can be considered as quasi isotropic (Gnaba et al., 2018). Still, depending on the manufacturing method and especially with carding process, they can highlight preferred orientations (Miao and Shan, 2011; Russell, 2007). Also, during a mechanical loading, fibres will be loaded differently depending on the orientation distribution. Due to their structure, flax fibres highlight high anisotropic properties and longitudinal, transverse and shearing properties of flax elementary and technical fibres (bundles) (Baley et al., 2006;

2

52 Thomason et al., 2017) that could greatly influence the overall composite's behaviour

53 and properties (Gager et al., 2019; Merotte et al., 2018).

54 Through research work around the world, there is now a good knowledge based on

55 nonwoven composites, particularly in terms of the influence of the type of

56 reinforcement, their microstructure and their various properties (Martin et al., 2016;

57 Merotte et al., 2016; Mieck et al., 1996). However, to allow optimised structural and

58 semi-structural applications, modelling and designing tools of these materials are

59 required. In terms of modelling mechanical properties, one of the major challenges to be

60 addressed is the implementation of fibre orientation and curvature. To do this, it is

61 necessary to rely on trusted data that can only be determined experimentally from

62 existing preforms.

63 Several studies have focused on the determination of the fibre orientation distribution

64 for various materials including fabrics, paper or fibre reinforced polymers. Acquisition

65 of images with digital cameras, optical, electronic or confocal microscopes are the most

66 commonly used (Enomae et al., 2006; Erdman et al., 2016; Koh and Madsen, 2018).

67 Miao and Shan (Miao and Shan, 2011) have studied the relationship between fibre

68 orientation and mechanical properties of flax nonwoven composites thanks to optical

69 microscopy imaging and then analysis Fiji® image processing software. Other methods

70 such as ultrasound scanning and X-ray Computed tomography were used by Smith et al.

71 to create 3D representations of carbon fibre composite plates (Smith et al., 2015). From

72 synchrotron radiation-based micro-computer tomography, Graupner et al. (Graupner et

73 al., 2016, 2014) characterised the fibre orientation of cellulose fibre-reinforced

74 polylactide composites by analysing the in-plane fibre orientations of several slices

75 through the thickness of the composite. All acquisition techniques can be justified

76 depending on the aim of the observation afterward. Indeed, different methods will allow

77 to get 2D or 3D images, characterise diverse surface areas from micro to macro scale,

78   with more or less precision and contrasts. Some techniques are also more suitable for

79   the analysis methods through which they will then be computed to determine the

80   orientation of the fibres (i.e. gray level or colour images) (Syerko et al., 2019).

81   Methods applicability must also be evaluated depending on the morphology of the

82   reinforcing fibres. Depending on the required performances and on their final use

83   application, composites can be reinforced with short or continuous fibres. For the first

84   category, the fibre orientation will mainly be a result of the flow of the suspension

85   within the polymer during the process. For long, continuous fibre composites, the

86   orientation will be given by the structure of the preform (i.e. woven fabrics, nonwoven

87   preforms etc..) as well as the structure of the long fibres which will govern their

88   straightness. Plant fibre reinforcement potentially being made of both bundles or

89   individual fibres (Baley et al., 2019); diameters are also of great importance. Thus, to be

90   consistent, fibre orientations quantification methods must correctly identify the

91   reinforcing elements (individual fibres, bundles) as well as their curvature and take the

92   fibre morphological characteristics (diameter and length) into account.

93   The main method used to determine the fibre orientation distribution in long fibre

94   reinforced composites is the Fast Fourier Transform (FFT) whose efficiency is

95   discussed in the literature (Ghassemieh et al., 2002; Pourdeyhimi and Kim, 2002). Due

96   to the periodic character of the Fourier transformation, this method is useful to describe

97   regular patterns in woven fabric where information is concentrated in the Fourier

98   spectrum in the vertical or horizontal direction, respectively. In contrast, purely random

99   orientation of fibres causes the frequency components in the power spectrum to be

100   approximately isotropic and possess a nearly circular shape (Yousfani et al., 2012).

101   Tunák et al. (Tunák et al., 2014; Tunák and Antoch, 2018) highlighted that the "global"

102   approach commonly used was not suitable enough to analyse nonwoven textiles or

103   nanofibrous layers, which often present non-homogeneity as well as anisotropy, and that

4

Other methods such

as the stereological method can be used; the composite is observed in its crossed

direction and the orientation of a circular fibre is determined from the ratio of the

ellipse formed by the orientation of a fibre (Eberhardt and Clarke, 2001; Jeon et al.,

2014; Yurgartis, 1987). This method does work for circular diameter fibre such as a

glass fibre but it cannot be applied to plant fibres which present complex heterogeneous

structures. Furthermore, as it is only at one location in the in-plane direction, curvature

of the fibre cannot be determined. Local gradient orientation method can also be used

but this way is questionable as only fibre edges are detected by filtering operators which

means fibre widths are not taken into account and this is a predominant information

when dealing with plant fibres. Other methods such as structure tensor (Krause et al.,

2010; Van Kempen et al., 1999) or mean intercept length (Luo et al., 1991; Sander and

Barocas, 2009) methods were also applied on composite materials and each of them has

its own benefits and drawback from the complexity to the accuracy of the method

(Syerko et al., 2019).

Despite their applicability to analyse composite materials, the methods previously

enounced are usually programmed in operating systems/software for which it is not

possible to manage settings such as the time of calculation and the accuracy of the

results. Also, depending on the applications, there is a need of a method where such

5

131 parameters can be managed. For scientific matters, the accuracy of the results is

132 prevalent. From an industrial point of view, a method quantifying the fibre orientation

133 in a preform directly after the production in order to control its conformity might be of

134 great interest. For this purpose, even if accuracy is important, the time of calculation is a

135 predominant factor if there is a large area to analyse. Moreover, by developing a method

136 for which there is a full understanding of the protocol, it is easier for the developers to

137 modify calculation algorithms to make them more efficient according to the material

138 characteristics.

139 This paper presents an original method based on gray-level granulometry to analyse the

140 fibre orientation distribution of both synthetic and flax preforms for composite

141 reinforcement. After a validation of the method developed on glass fibres unidirectional

142 (UD) and nonwoven preforms, results obtained with similar flax fibre preforms are

143 shown and discussed.

144 **2. Materials and methods**

145 2.1 Materials

146 Flax (*Linum usitatissimum*) tows and scutched fibres grown in Normandy (France) were

147 used to produce the nonwoven and the unidirectional tape (Martin et al., 2014). Natural

148 fibre nonwovens were manufactured according to the carding/over-lapping/needle

149 punching technology (Russell, 2007) whereas the unidirectional tape is produced by a

150 specific process well described by Khalfallah et al. (Khalfallah et al., 2014). The

151 materials (i.e. nonwoven and UD tape), coming from Eco-Technilin SAS®, have an

152 areal weight of respectively 70 g.m^{-2} and 110 g.m^{-2}, respectively. E-Glass fibre mat and

153 unidirectional fabric made respectively following air blowing (Russell, 2007) and

154 weaving technologies were also studied to validate the method. They were supplied by

155 Composite Distribution and have both an areal weight of 200 g.m^{-2}. The unidirectional

156 fabric is not a pure UD fabric as it presents a few fibres in the weft direction (weight

157 fraction around 0.4%). Names and properties related to the different preforms are given

158 in table 1.

159 **Table 1. Characteristics of the various preforms analysed.**

Name	Type	Fibre type	Areal weight (g/m^2)	Preform thickness (µm)	Fibres/bundles length (mm)	Preferred orientation (°)
Flax UD	Unidirectional	Flax	70	150 ± 20	Bundles assembly	Longitudinal
Flax NW	Nonwoven	Flax	110	200 ± 10	50-200	Cross direction (CD)
Glass UD	Unidirectional	Glass	200	190 ± 20	continuous	Longitudinal
Glass mat	Nonwoven	Glass	200	460 ± 40	40-70	None

160

161   2.2   Scanning Electronic Microscope Imaging

162 SEM observations were performed on glass and flax preforms. Rectangular samples

163 (60x40 mm) were sputter-coated with a thin layer of gold in an Edwards Sputter Coater

164 and analysed with a Jeol JSM 6460LV SEM at 20 kV.

165   2.3   Images Analysis Methodology

166 Images were analysed by computing the histogram of the preferred orientation of pixels.

167 The preferred orientation is computed by applying gray-level granulometry curves with

168 various orientations, computing a typical size in each direction, and estimating the

169 preferred orientation from typical sizes.

170 **Figure 1.**

171 Gray-level granulometry is an approach for image texture analysis based on the

172 application of morphological filters (typically opening or closing) of increasing size

173 (Devaux et al., 2008; Soille, 2003). Gray-level morphological opening is an operation

174 that removes bright structures that are smaller than the structuring element. Let us denote

175 by $\gamma_B(I)$ the result of morphological opening with structuring element B_λ of size λ on the

176 image I. The computation of granulometry involves a family of structuring elements

177 $\{B_{\lambda_i}\}_{i=1,\ldots,n}$ of increasing sizes λ_i. The result obtained with each size λ_i is summarised by

178 the image volume curve V_i, that corresponds to the sum of the gray level values in the

179 corresponding result of opening. The derivative of the image volume curve results in

180 granulometric curves that can be interpreted in terms of size distribution:

181
$$G_i = \frac{V_{i+1} - V_i}{V_\infty - V_0}$$

182 Figure 1 presents an example of granulometric curve computed on a sample image of a

183 flax fibres nonwoven. A peak can be noticed around 5 pixels, that corresponds to the

184 thickness of the majority of fibres visible in image. Another peak can be noticed around

185 15 pixels, corresponding to thicker fibres. The corresponding fibres are visible on the top

186 images.

187 A granulometric curve can be summarised by a gray-level mean size that depicts the

188 typical size of the structures within the image. The geometrical mean $m_G =$

189 $\exp[\sum_i \log \lambda_i \, G_i]$ was considered, which resulted in values closer to the centre of the peak

190 than the mean or the median (Devaux et al., 2008).

191 Gray-level granulometry is typically computed using structuring elements with square or

192 disk shapes. In order to assess the preferred orientation of texture, linear structuring

193 elements with various orientations may be used (Devaux et al., 2008; Legland et al.,

194 2012; Soille, 2003). Families of linear structuring elements were considered; they are

195 obtained by identifying the pixels around the line with orientation θ containing the origin,

196 and keeping the number of pixels that best approximates the expected length. The

197 computation of granulometric curves on the whole image using linear structuring

198 elements with various orientations results in a granulometric curve for each orientation.

199 The computation of geometric means results in a function $m_G(\theta)$ that depicts the typical

200 size depending on the orientation.

201 **Figure 2.**

202 In order to compute preferred orientation for a given pixel, it is necessary to compute

203 locally (i.e. for each pixel) the functions $m_G(\theta)$. In practice, this requires to replace the

204 computation of global image volumes V_i by their local counterparts $V_i(x, \theta)$, where x

205 corresponds to the pixel position and θ corresponds to the orientation. Resulting

206 granulometric curves $G_i(x, \theta)$ can be summarised by computing for each pixel and for

207 each orientation the local oriented gray-level mean size $m_G(x, \theta)$. Fig. 2.B and Fig. 3.C

208 show examples of local gray-level mean size maps for orientations corresponding to 0,

209 45, 90, and 135 degrees computed on a synthetic image (Fig. 2.A) and on a cropped

210 image of flax fibres (Fig. 3.A). The elongated regions result in a large mean size value

211 when the orientation corresponds to the orientation of elongation.

212 For each pixel, the function $m_G(x, \theta)$ exhibits one or several maxima for orientations

213 corresponding to the presence of fibre. Fig. 2.C represents this function for point located

214 in a vertically oriented region, shown as a red cross in Fig. 2.A. The best orientation

215 $\theta^*(x)$, corresponding to the most prominent fibre direction for the pixel x, is computed

216 by integrating the function $m_G(x, \theta)$ over the circular domain $[0; 2\pi[$. The resulting map

217 of orientation is represented using a colour map depending on the orientation: the red

218 colour corresponds to a horizontal orientation, and the light blue colour corresponds to a

219 vertical orientation (Fig. 2.D).

220 The estimate of local orientation is computed for all pixels. However, as the dark pixels

221 correspond to background, it is relevant to consider only the orientation of the bright

222 pixels. Therefore, parametric maps of local orientation are represented using a colour

223 coding that takes into account both the orientation and the local intensity of the pixel

224 (Fig. 3.C). For the same reason, the histogram of preferred orientations is obtained by

225 computing the histogram of the values $\theta^*(x)$ weighted by $I(x)$, the intensity of x in the

226 original image (Fig. 3.D).

227 **Figure 3.**

228

3. Results and discussion

3.1 Validation of the method

231 This method was originally developed to estimate the fibre orientation distribution (FOD)

232 of flax fibre nonwovens. These materials can be considered as complex materials. Indeed,

233 in the stem, flax fibres are arranged in bundles and are then more or less individualised

234 during the processes they undergo (retting, scutching, carding, etc.) resulting in individual

235 fibres and bundles with heterogeneous diameters and lengths. Also, flax fibres and

236 bundles are flexible enough to bend and therefore, the analysis is more complicated than

237 if the fibres remained straight as it is the case for glass fibre.

238 **Figure 4.**

239 For all these reasons, the method is validated with more conventional materials before

240 testing flax fibre webs. Figure 4 A, B and C show SEM images of three reference

241 materials: Glass fibre mat, glass fibre UD fabric and UD flax tape, respectively. The

242 computed preferred orientation maps are also represented in Figure 4 D, E and F where a

243 colour represents an orientation; thus, a random orientation is presumed to give a large

244 range of colours whereas a reduced colour shade is expected when a unidirectional

245 preform is analysed. The trends shown in Figures 4 D, E and F are clearly in this

246 direction and are confirmed with the results shown in Fig.4 G). Indeed, the glass fibre

247 mat FOD exhibits a quasi-monotonous line fluctuating between 0.4 and 1% highlighting

248 the random in-plane orientation of fibres. On the contrary, glass fibre unidirectional

249 fabric FOD shows a thin peak between orientations ranging from 80 to 100° and displays

250 a maximum value at 89° (longitudinal axis). If the curve is compared with the one of flax

251 fibre unidirectional tape, the peak is higher and thinner. Indeed, for flax, a peak is also

252 present with a maximum at 90° but it only represents 5% of the fibres (13% for glass) and

253 it is also more scattered with orientations ranging from 75° to 105°. As glass

254 reinforcement is made of continuous individual fibres assembled in 2 mm wide bundles,

255 it is less likely to bend due to its higher moment of inertia compared to flax individual

256 fibres and bundles (Tanguy et al., 2018), with diameters varying from 15 to 100 µm

257 (Charlet et al., 2010; Haag and Müssig, 2016). Also, bundles may have been damaged

258 during the mechanical scutching process and the manufacturing process of unidirectional

259 flax tapes (Khalfallah et al., 2014), where some individual fibres can break up from the

260 bundle and become disoriented, this is visible on Fig. 4.C and 4.F) with some small

261 diameter bent fibres. On this point it should be kept in mind that the production of flax

262 fibre reinforcements is a much more complex process than for glass fibres; the glass

263 fibres are extruded and calibrated in an industrial way then directly assembled into roving

264 and preforms. In the case of flax, they are mechanically extracted from a plant, then

265 aligned and ribboned with all the risks involved in these successive operations, with new

266 possibilities for creating defects at each stage.

267 From figure 4. F. it can be observed that on large flax fibre bundles, there is a variation in

268 colour for the same element that can be explained by the fact that the method detects

269 elements crossing each other and for the area where fibres are overlapping, it gives a

270 mean orientation of these later. Also, if the fibres are too wide, the method can hardly

271 recognize them as a single element and thus it gives two symmetric orientations for this

272 element. This later can be resolved by adjusting the image analysis settings with the

273 increase of the morphological filter size which will give a more accurate result but needs

274 a longer time to process.

275   3.2   Application to flax fibre nonwoven preforms

276   **Figure 5.**

277 Similar analyses were performed on flax nonwoven (Figure 5). Referring to the fibre

278 orientation distribution curves, there is a preferred orientation around 90°. This was not

279 reported for glass fibre mats (Fig. 4.G) and this phenomenon can be explained by the

11

280 manufacturing process of nonwovens which are different for the two materials. Indeed,

281 the glass fibre mat studied here is made by air blowing where fibres are randomly

282 dispersed in the plane whereas flax fibre nonwovens were produced by carding

283 technology with a roller card; fibres are conveyed by several rolls to be disentangled and

284 mixed in order to form homogeneous web of uniform weight per unit area. Fibres are thus

285 more oriented in the machine direction (Van De Velde and Kiekens, 2003). During the

286 overlapping step, the web is reoriented almost perpendicularly to the machine direction

287 allowing a preferred orientation in the cross direction (CD) (90° in figure 5 and 6). Same

288 observations as for unidirectional flaxtape with the fibres overlapping each other can be

289 reported for nonwovens.

290   **Figure 6.**

291 Fig. 6 represents an analysis of the fibre orientation distribution for four different

292 locations on the nonwoven. Trends are found to be quite similar for areas 1, 2 and 3 with

293 a preferred orientation at 90° whereas for the fourth location, the peak is wider and

294 shifted to 70° values and this is likely due to the size of the analysed area. The

295 observation scale is a key point for the accurate analysis of the fibre orientation

296 distribution because if the latter is too small then there are not enough fibres analysed and

297 the distribution thus obtained will not be representative of that of the whole material. On

298 the contrary, if it is too large, the smallest elements may not be detected due to a lack of

299 image quality, leading to an error in determining the orientation of the fibres. With the

300 magnification used here, smaller diameter fibres are detected and by analysing over

301 several areas, it is possible to obtain a precise and representative fibres orientation

302 distribution within the nonwoven. By automating the image analysis, it would then be

303 possible to analyse a very large surface of a sample that can then be mechanically tested

304 and thus verify the actual orientation distribution of the fibres and the impact this will

305 have on the mechanical properties; on the other hand, these data could make it possible to

306 implement a mathematical model to predict the properties of nonwoven composites

307 reinforced by plant fibres. Particular attention should be paid to the fact that with this

308 method, only a surface analysis is performed. This corresponds well for so-called

309 lightweight preforms since the majority of the fibres are analysed here. That said, the

310 increase in weight will affect the thickness of the preform with more fibres in the

311 background that may not have the same orientation as those analysed. Additionally, in the

312 special case of needle-punched nonwovens with higher thickness, the needle punching

313 step drives few fibres through the thickness of the material resulting in a three-

314 dimensional orientation of the fibres. From these points, a three-dimensional image

315 acquisition method and analysis may be required to ensure a reliable fibre orientation

316 characterisation on the entire material.

317

318 **4. Conclusion**

319 This paper presents a new method to analyse the fibre orientation distribution (FOD) of

320 both synthetic and flax preforms for composite reinforcement. Preforms images were

321 obtained by scanning electronic microscopy (SEM) and analysed by computing the

322 histogram of pixels preferred orientations by using gray-level granulometry. Gray-level

323 granulometry is an approach for image texture analysis based on the application of

324 morphological filters (typically opening or closing) of increasing size which results in

325 granulometric curves that can be interpreted in terms of size distribution. The method

326 computes a parametric map of local orientation using a colour coding taking into account

327 both the orientation and the local intensity of the pixel. It also gives a histogram

328 representing the preferred orientations of the analysed elements.

329 Originally developed for flax fibre nonwovens, the method is first validated with more

330 conventional materials such as unidirectional glass fabric, UD flax tapes as well as glass

331 fibre mat. The results obtained are in accordance with those expected with significant

332 differences between the FOD of the different preforms highlighting the influence of

333 parameters such as the intrinsic characteristics of the materials and their production

334 methods. Similar analyses were performed on different locations of a flax nonwoven

335 which highlighted a preferred orientation around 90°. Due to the reduced size of the

336 analysed area, it is necessary to process to image analysis on different location and

337 arithmetically average the values to assure reliable material fibre orientation distribution.

338 This method could be combined with several image acquisition techniques (SEM,

339 tomography) both at the preform and composite level offering a large range of

340 applications including composite materials. Potential improvements of the method can be

341 imagined with the quantification fibres and bundles diameters or determination of the

342 orientation in the three dimensions. Finally, it provides interesting perspectives for

343 numerical modelling of biocomposite mechanical properties.

344

348

349 **References**

350 Baley, C., Goudenhooft, C., Perré, P., Lu, P., Pierre, F., Bourmaud, A., 2019.
351   Compressive strength of flax fibre bundles within the stem and comparison with
352   unidirectional flax/epoxy composites. Ind. Crop. Prod. 130, 25–33.
353   https://doi.org/10.1016/j.indcrop.2018.12.059

354 Baley, C., Perrot, Y., Busnel, F., Guezenoc, H., Davies, P., 2006. Transverse tensile
355   behaviour of unidirectional plies reinforced with flax fibres.
356   https://doi.org/10.1016/j.matlet.2006.02.028

357 Bourmaud, A., Beaugrand, J., Shah, D.U., Placet, V., Baley, C., 2018. Towards the design
358   of high-performance plant fibre composites: How can we best define the diversity
359   and specificities of plant cell walls? Prog. Mater. Sci. 97, 347–408.

https://doi.org/10.1016/j.pmatsci.2018.05.005

Charlet, K., Jernot, J.P., Eve, S., Gomina, M., Bréard, J., 2010. Multi-scale morphological characterisation of flax: From the stem to the fibrils. Carbohydr. Polym. 82, 54–61. https://doi.org/10.1016/j.carbpol.2010.04.022

Devaux, M.F., Bouchet, B., Legland, D., Guillon, F., Lahaye, M., 2008. Macro-vision and grey level granulometry for quantification of tomato pericarp structure. Postharvest Biol. Technol. 47, 199–209. https://doi.org/10.1016/j.postharvbio.2007.06.017

Eberhardt, C., Clarke, A., 2001. Fibre-orientation measurements in short-glass-fibre composites . Part I : automated , high-angular-resolution measurement by confocal microscopy 61, 1389–1400.

Enomae, T., Han, Y.-H., Isogai, A., 2006. Nondestructive determination of fiber orientation distribution of paper surface by image analysis. Nord. Pulp Pap. Res. J. 21, 253–259. https://doi.org/10.3183/NPPRJ-2006-21-02-p253-259

Erdman, A., Grzyb, T., Kulpinski, P., Lazarek, J., Lis, S., Olejnik, K., Reczulski, M., Szczepaniak, P.S., Wysocka-robak, A., 2016. Estimation of Fibre Orientation in Paper Products by an Image Analysis On-line System 2, 107–112. https://doi.org/10.5604/12303666.1191435

Gager, V., Le Duigou, A., Bourmaud, A., Pierre, F., Behlouli, K., Baley, C., 2019. Understanding the effect of moisture variation on the hygromechanical properties of porosity-controlled nonwoven biocomposites. Polym. Test. 78, 105944. https://doi.org/10.1016/j.polymertesting.2019.105944

Ghassemieh, E., Acar, M., Versteeg, H., 2002. Microstructural analysis of non-woven fabrics using scanning electron microscopy and image processing. Part 1: development and verication of the methods. Proc. IMechE, Part L J. Mater. Des. Appl. 216, 199–207.

Gnaba, I., Omrani, F., Wang, P., Soulat, D., Ferreira, M., Vroman, P., Jaouachi, B., 2018. Mechanical behavior of flax/polypropylene commingled nonwoven at dry scale: Influence of process parameters. Text. Res. J. 004051751875578. https://doi.org/10.1177/0040517518755789

Graupner, N., Beckmann, F., Wilde, F., Müssig, J., 2014. Using synchroton radiation-based micro-computer tomography (SR µ-CT) for the measurement of fibre orientations in cellulose fibre-reinforced polylactide (PLA) composites. J. Mater. Sci. 49, 450–460. https://doi.org/10.1007/s10853-013-7724-8

Graupner, N., Ziegmann, G., Wilde, F., Beckmann, F., Müssig, J., 2016. Procedural influences on compression and injection moulded cellulose fibre-reinforced polylactide (PLA) composites: Influence of fibre loading, fibre length, fibre orientation and voids. Compos. Part A Appl. Sci. Manuf. 81, 158–171. https://doi.org/10.1016/j.compositesa.2015.10.040

Haag, K., Müssig, J., 2016. Scatter in tensile properties of flax fibre bundles: influence of determination and calculation of the cross-sectional area. J. Mater. Sci. 51, 7907–7917. https://doi.org/10.1007/s10853-016-0052-z

Jeon, S.-Y., Yu, W.-R., Kim, M.S., Lee, J.S., Kim, J.W., 2014. Predicting the tensile strength of needle-punched nonwoven mats using X-ray computed tomography and a statistical model. Fibers Polym. 15, 1202–1210. https://doi.org/10.1007/s12221-014-1202-z

15

Jones, R.M., 1999. Mechanics of composite materials. Mech. Compos. Mater. https://doi.org/10.1007/BF00611782

Khalfallah, M., Abbès, B., Abbès, F., Guo, Y.Q., Marcel, V., Duval, A., Vanfleteren, F., Rousseau, F., 2014. Innovative flax tapes reinforced Acrodur biocomposites : A new alternative for automotive applications. J. Mater. 64, 116–126. https://doi.org/10.1016/j.matdes.2014.07.029

Koh, R., Madsen, B., 2018. Strength failure criteria analysis for a flax fibre reinforced composite. Mech. Mater. 124, 26–32. https://doi.org/10.1016/j.mechmat.2018.05.005

Kratmann, K.K., Sutcliffe, M.P.F., Lilleheden, L.T., Pyrz, R., Thomsen, O.T., 2009. A novel image analysis procedure for measuring fibre misalignment in unidirectional fibre composites. Compos. Sci. Technol. 69, 228–238. https://doi.org/10.1016/j.compscitech.2008.10.020

Krause, M., Hausherr, J.M., Burgeth, B., Herrmann, C., Krenkel, W., 2010. Determination of the fibre orientation in composites using the structure tensor and local X-ray transform. J. Mater. Sci. 45, 888–896. https://doi.org/10.1007/s10853-009-4016-4

Legland, D., Devaux, M.F., Bouchet, B., Guillon, F., Lahaye, M., 2012. Cartography of cell morphology in tomato pericarp at the fruit scale. J. Microsc. 247, 78–93. https://doi.org/10.1111/j.1365-2818.2012.03623.x

Luo, G.M., Sadegh, A.M., Cowin, S.C., 1991. The mean intercept length polygons for systems of planar nets. J. Mater. Sci. 26, 2389–2396. https://doi.org/10.1007/BF01130186

Martin, N., Davies, P., Baley, C., 2016. Evaluation of the potential of three non-woven flax fiber reinforcements: Spunlaced, needlepunched and paper process mats. Ind. Crops Prod. 83, 194–205. https://doi.org/10.1016/j.indcrop.2015.10.008

Martin, N., Davies, P., Baley, C., 2014. Comparison of the properties of scutched flax and flax tow for composite material reinforcement. Ind. Crops Prod. 61, 284–292. https://doi.org/10.1016/j.indcrop.2014.07.015

Merotte, J., Le Duigou, A., Bourmaud, A., Behlouli, K., Baley, C., 2016. Mechanical and acoustic behaviour of porosity controlled randomly dispersed flax/PP biocomposite. Polym. Test. 51, 174–180. https://doi.org/10.1016/j.polymertesting.2016.03.002

Merotte, J., Le Duigou, A., Kervoelen, A., Bourmaud, A., Behlouli, K., Sire, O., Baley, C., 2018. Flax and hemp nonwoven composites: The contribution of interfacial bonding to improving tensile properties. Polym. Test. 66, 303–311. https://doi.org/10.1016/j.polymertesting.2018.01.019

Miao, M., Shan, M., 2011. Highly aligned flax/polypropylene nonwoven preforms for thermoplastic composites. Compos. Sci. Technol. 71, 1713–1718. https://doi.org/10.1016/j.compscitech.2011.08.001

Mieck, K.-P., Lützkendorf, R., Reussmann, T., 1996. Needle-Punched hybrid nonwovens of flax and ppfibers—textile semiproducts for manufacturing of fiber composites. Polym. Compos. 17, 873–878. https://doi.org/10.1002/pc.10680

Pourdeyhimi, B., Kim, H.S., 2002. Measuring Fiber Orientation in Nonwovens: The Hough Transform. Text. Res. J. 72, 803–809. https://doi.org/10.1177/004051750207200909

451 Russell, S.J., 2007. Handbook of nonwovens. Woodhead Publishing Limited.

452 Sander, E.A., Barocas, V.H., 2009. Comparison of 2D fiber network orientation
453 measurement methods. J. Biomed. Mater. Res. - Part A 88, 322–331.
454 https://doi.org/10.1002/jbm.a.31847

455 Shah, D.U., Schubel, P.J., Clifford, M.J., 2013. Can flax replace E-glass in structural
456 composites? A small wind turbine blade case study. Compos. Part B Eng. 52, 172–
457 181. https://doi.org/10.1016/j.compositesb.2013.04.027

458 Smith, R.A., Nelson, L.J., Xie, N., Fraij, C., Hallett, S.R., 2015. Progress in 3D
459 characterisation and modelling of monolithic carbon-fibre composites. Insight Non-
460 Destructive Test. Cond. Monit. 57, 131–139.
461 https://doi.org/10.1784/insi.2014.57.3.131

462 Soille, P., 2003. Morphological Image Analysis. Springer.

463 Syerko, E., Oter, L., Pawar, A., Binetruy, C., Advani, S.G., Eck, B., 2019. Comparative
464 Study of Methods for the Quantification of Fiber Orientations of Composite
465 Reinforcements, in: 21ème Journées Nationales Sur Les Composites - JNC 21.
466 Bordeaux, pp. 1–9.

467 Tanguy, M., Bourmaud, A., Beaugrand, J., Gaudry, T., Baley, C., 2018. Polypropylene
468 reinforcement with flax or jute fibre; Influence of microstructure and constituents
469 properties on the performance of composite. Compos. Part B Eng. 139, 64–74.
470 https://doi.org/10.1016/j.compositesb.2017.11.061

471 Thomason, J., Yang, L., Gentles, F., 2017. Characterisation of the Anisotropic
472 Thermoelastic Properties of Natural Fibres for Composite Reinforcement. Fibers 5,
473 1–12. https://doi.org/10.3390/fib5040036

474 Tunák, M., Antoch, J., 2018. Monitoring homogeneity of textile fiber orientation. Text.
475 Res. J. 88, 1226–1243. https://doi.org/10.1177/0040517517698983

476 Tunák, M., Antoch, J., Kula, J., Chvojka, J., 2014. Estimation of fiber system orientation
477 for nonwoven and nanofibrous layers: Local approach based on image analysis.
478 Text. Res. J. 84, 989–1006. https://doi.org/10.1177/0040517513509852

479 Van De Velde, K., Kiekens, P., 2003. Effect of Flax/PP Panel Process Parameters on
480 Resulting Composite Properties. J. Thermoplast. Compos. Mater. 16, 413–431.
481 https://doi.org/10.1177/0892705703031637

482 Van Kempen, G.M.P., Van den Brink, N., Van Vliet, L.J., Van Ginkel, M., Verbeek,
483 P.W., Blonk, H., 1999. The application of a Local Dimensionality Estimator to the
484 analysis of 3-D microscopic network structures, in: Proceedings of the 11th
485 Scandinavian Conference on Image Analysis, Kangerlussuaq, Greenland. pp. 447–
486 455.

487 Yousfani, S.H.S., Gong, R.H., Porat, I., 2012. Manufacturing of Fibreglass Nonwoven
488 Webs Using a Paper Making Method and Study of Fibre Orientation in These Webs.
489 Fibres Text. East. Eur. 91, 61–67.

490 Yurgartis, S.W., 1987. Measurement of small angle fiber misalignments in continuous
491 fiber composites. Compos. Sci. Technol. 30, 279–293. https://doi.org/10.1016/0266-
492 3538(87)90016-9

493

494 **Figure captions**

495 **Figure 1.** Computation of granulometric curves using morphological opening. Top row:

496 sample results of morphological opening using square structuring elements of increasing

497 sizes. Bottom: resulting granulometric curve. The dots on the curve correspond to the

498 stages shown on the first row.

499 **Figure 2.** Computation of preferred orientation map on a synthetic image. A) Original

500 image. B) Results of local mean size for different families of linear structuring element

501 oriented with 0, 45, 90 and 135 degrees. C) Mean size function for a single pixel and the

502 whole range of orientations. D) Synthetic map of preferred orientation represented using

503 colour.

504 **Figure 3.** Computation of local orientation map from granulometry curves obtained by

505 analysis on a flax nonwoven. A) Original image (inverted) B) Granulometric size

506 obtained with various orientations of structuring elements C) Colour representation of

507 preferred orientation map. D) Histogram of preferred orientations.

508 **Figure 4.** Original SEM images of A) glass fibre mat, B) glass fibre unidirectional

509 preform and C) flax fibre unidirectional tape. D), E) and F) are the computed preferred

510 orientation maps of glass fibre mat, glass UD and flax UD, respectively. G) is the

511 comparison of the fibre orientation distribution (FOD) of the preforms.

512 **Figure 5.** Original SEM image of flax fibres nonwoven A). B) is the computed preferred

513 orientation maps of A) and C) shows the histogram representing the fibre orientation

514 distribution.

515 **Figure 6.** Original SEM image of a larger area of flax fibres nonwoven divided in four

516 areas A). The histogram represents the fibre orientation distribution of each area analysed
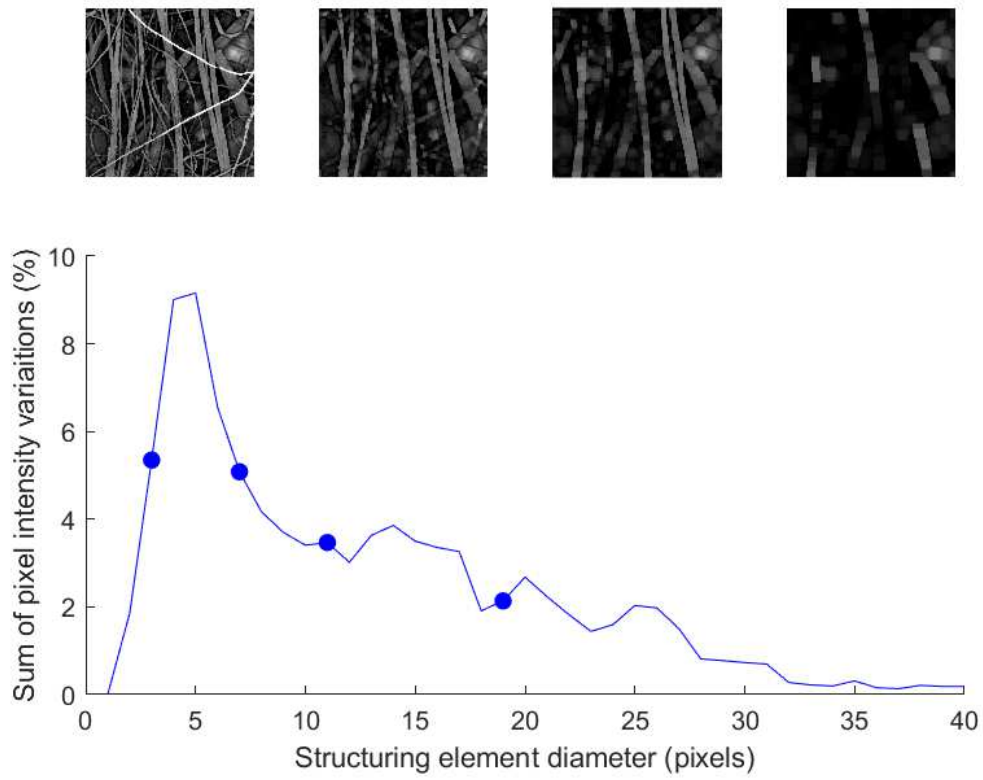
517 B).
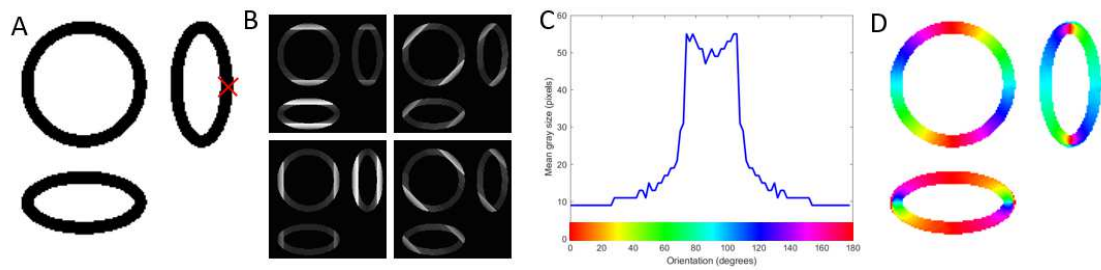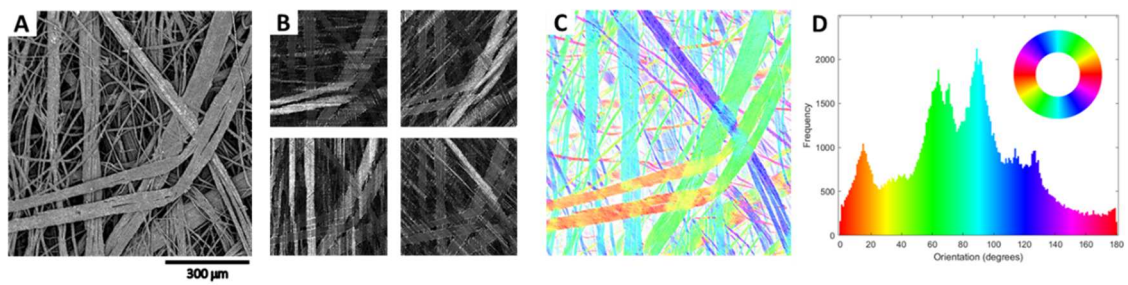
518

Figure 1.
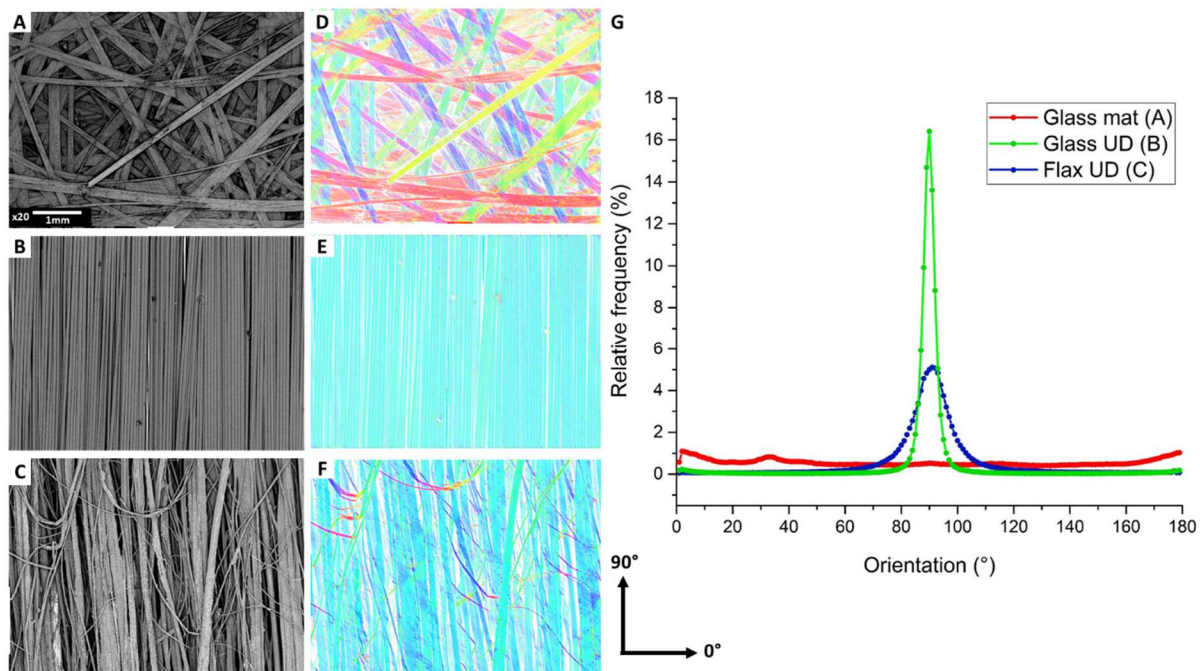

Figure 2.

Figure 3.

Figure 4.

Figure 5.

Figure 6.